CROATICA CHEMICA ACTA
CCACAA **80** (3-4) 503–515 (2007)
ISSN-0011-1643
CCA-3193
Original Scientific Paper

Ageing in the Inorganic Nanoworld: Example of Magnetite Nanoparticles in Aqueous Medium*

Etelka Tombácz, Erzsébet Illés, Andrea Majzik, Angéla Hajdú, Nóra Rideg, and Márta Szekeres**

Department of Colloid Chemistry, University of Szeged, H-6720 Szeged, Aradi Vt. 1. Hungary

RECEIVED DECEMBER 30, 2006; REVISED MAY 23, 2007; ACCEPTED JUNE 4, 2007

Changes in the inherent solid phase and aqueous interfacial properties of magnetite nanoparticles in a Massart type magnetic fluid were investigated. Magnetite nanoparticles were synthesized, purified, dialyzed against 0.001 mol dm^{-3} HCl and then stored at 4 °C for 6 years. The solid phase transformation of magnetite to maghemite and formation of akageneite shell on the magnetic core, as well as a slight increase in particle size were proved, causing no change in the superparamagnetic features of nanoparticles after storage as long as 6 years. The aqueous interfacial properties, however, were altered in a strange way. Surprisingly, neither the surface charge density nor the particle charge in acidic region showed significant changes, except for a definite decrease in pH_{pzc} and pH_{iep} from pH ≈ 8 to ≈ 7. Coalescence of akageneite shell during recrystallization resulted in a significant decrease of the specific surface area of the aged sample, and probably contributed to its declining colloidal stability.

Keywords
magnetic fluids
pH-dependence
surface charging
solubility
recrystallization
colloidal stability

INTRODUCTION

Ageing is a universal process in nature. Not only living creatures change continuously along an irreversible way, but several examples can also be found in the inorganic world. It is a well-known phenomenon in colloid science[1–4] and has been studied from its beginning.[5] The ageing of colloidal dispersions, often referred to as Ostwald ripening, is inherently involved in their stability, since they are not stable from the thermodynamic point of view due to the high surface excess free energy. The latter is proportional to the surface area present in the given dispersion and greatly increases as the size of dispersed particles decreases.[2] Thus, the significance of this ageing process, taking place spontaneously with time, becomes more and more evident with decreasing particle size, especially in the subcolloidal region, *i.e.,* over the lowest (up to 50 nm) size range, the realm of the recently favored nanoparticles. There are several unknown interrelations, specific expressions and questions related to ageing in the inorganic nanoworld. In general, a more stable crystalline phase is reached and the particles grow because of the size dependent solubility of solid particles, well-known from the old work[5] of Ostwald: $\ln (c(r)/c_\infty) = 2V_S \gamma/RTr$, where $c(r)$ is the solution concentration in equilibrium with particles of radius r and c_∞ is the bulk solubility, V_S is the molar volume, γ is the surface free energy at solid/liquid interface, R is the gas constant and T is the temperature. It is not questionable that these processes result in slower or faster changes in the colloidal state. How-

* Dedicated to Professor Nikola Kallay on the occasion of his 65th birthday.

** Author to whom correspondence should be addressed. (E-mail: tombacz@chem.u-szeged.hu)

ever, the question is how the structure of the inherent solid phase and of the surface alters during ageing and what is their effect on the interfacial properties. Both inner and surface crystallization may take place, so both the solid phase bulk properties and the morphology of particles probably change. The altering interfacial properties in aqueous dispersions, which contribute to the change in their colloidal stability in a somewhat unexpected way, are of particular interest.

Perhaps the most interesting compounds in the inorganic nanoworld are iron oxides, not only because of their abundance in nature and variability in crystalline form, but also owing to the multidisciplinary nature of iron oxide research involving geobiochemical processes, soil and environmental sciences, importance in life processes, biomedical application and industrial technology. A wide variety of iron oxides[6–8] (*e.g.,* hematite, goethite, ferrimagnetic magnetite, maghemite, *etc.*) occur in nature. Every ferrimagnetic material has a net magnetic moment, and is strongly attracted by a magnetic field. These substances have a domain structure and only particles in the nanosize range consist of a single domain. Iron oxide particles with different crystal structures usually exist as colloidal particles (*e.g.,* ferrihydrite ≈ 5–10 nm, goethite, hematite ≈ 10–50 nm, magnetite ≈ 10 nm, maghemite ≈ 30–50 nm). The very small (< 10 nm) magnetite nanoparticles are superparamagnetic[8] (*i.e.,* rapid, spontaneous fluctuation between the spin states is allowed) at room temperature.

Nowadays, the complex fluids of magnetic nanoparticles are in the center of international interest.[9] The great interest in these materials is due to the possibilities of their different applications in electronics (*e.g.,* magnetic ink, recording media) and medicine (magnetic resonance contrast media, therapeutic agents in cancer treatment, *etc.*). Their biomedical application[10] is of especially great importance. Water based magnetic fluids (MFs) containing magnetic nanoparticles (*e.g.,* magnetite, maghemite) coated with biocompatible or functionalized layer are used in magnetic hyperthermia, drug targeting, cell separation, since they can be manipulated by an external magnetic field gradient, or as contrast enhancing agents in MRI. Besides several unique problems of particular applications, the colloidal stability of magnetic fluids, especially the slow processes during storage, *i.e.,* ageing of water based MFs, is critical. Enhanced solubility of magnetite nanoparticles (≈ 12 nm) producing dissolved Fe ions in aqueous medium above 0.0003 mol dm^{-3} concentration, especially below pH ≈ 4, has been proved[11] without mentioning the classical Ostwald law on particle size dependent solubility of colloidal particles, which is particularly significant in the nanosize region (up to 50 nm), though the paper was published in one of the best colloidal journals. In a recent study,[12] the solid phase transition of (γ-Fe_2O_3) nanoparticles from magnetite to maghemite was implemented by aeration oxidizing in acidic medium at ≈100 °C for an hour to obtain stable maghemite nanoparticles, which may be used in magnetic ferrofluid hyperthermia (MFH) applications because of their satisfactory heating properties in the ac magnetic field.

This work shows a specific example of ageing nanoparticles in aqueous medium. Electrostatically stabilized magnetite nanoparticles (Massart type water based magnetic fluid) were stored for six years. The ageing process was followed using several methods, since it involves slow crystallization, change in the inherent solid phase properties such as spontaneous transformation of magnetite mainly to maghemite, and morphological changes, along with a definite alteration of the aqueous interface expressed as surface and particle charge properties. The latter may be the reason for the great variety of the surface charge properties of magnetite published in literature.

EXPERIMENTAL

Materials

Magnetite nanoparticles were synthesized by alkaline hydrolysis[8,13,14] of iron(II)- and iron(III)-salts ($FeCl_2 \cdot 4H_2O$ and $FeCl_3 \cdot 6H_2O$, Reanal, Hungary). Concentrated solutions of iron(II)- and iron(III)-salts were mixed in a ratio of 1.1 to 2, and filtered into fresh Milli-Q water using microfilter 0.2 μm. The calculated amount of freshly prepared NaOH solution was added in 10 % excess to the doubly diluted iron-salt solution in two portions, the first half slowly and the second half suddenly under rigorous stirring. The formed black suspension was stirred for a few minutes, then transferred into a larger amount of Milli-Q water. The suspension was washed with water several times to eliminate alkaline impurities from the synthesis, then acidified with HCl solution down to pH ≈ 2, washed again with water until peptization, and finally dialyzed against 0.001 mol dm^{-3} HCl. Magnetite concentration was determined gravimetrically from the sample dried at 105 °C. The stock suspension (15.62 g magnetite in 100 g 0.001 mol dm^{-3} HCl) was stored in the dark at 4 °C.

All experiments were performed at room temperature (25 ± 1 °C). All reagents were of analytical grade, products of Reanal (Hungary), and Milli-Q water was used.

Methods

X-ray diffraction (XRD). – The XRD patterns of freshly prepared and aged iron oxides were taken using a Philips PW 1830/PW 1820 X-ray diffractometer operating in the reflection mode with Cu-Kα radiation. A copper sample holder was used. The scanning range was between 20 and 80 degrees of 2Θ. The probable phase transformation of magnetite nanoparticles during longer storage was followed; freeze-dried samples of freshly prepared, 3- and 6-year-old suspensions were studied. Identification of different iron

oxides was based on the position of characteristic peaks in the diffractograms using the JCPDS (Joint Committee on Powder Diffraction Standards) database.[8,11] The XRD patterns were evaluated determining the lattice spacings (d_{hkl} values) by the Bragg equation and the Miller (*hkl*) indices[15] corresponding to the crystalline phases present in the samples. The average particle size was calculated from the broadening of the diffraction peak corresponding to the most intensive reflection according to the JCPDS database. The Scherrer equation $d_{av} = K*\lambda/B*\cos\Theta$ was used,[16,17] where d_{av} is the average crystallite/particle size, K is the Scherrer constant (shape factor, its value is 0.9 for magnetite and maghemite,[7,12] λ is the X-ray wavelength (λ = 0.154 nm), B is the broadening related to the particle (difference between the measured width at half maximum of the diffraction peak (B_b) and the instrumental broadening of the single crystal form (B_s)), and Θ is the position of the diffraction peak maximum (B is given in radians).

Transmission Electron Microscopy (TEM). – TEM micrographs of iron oxide nanoparticles were taken using a Philips CM-10 transmission electron microscope supplied with a Megaview-II camera. The accelerating voltage of 100 kV was applied. The maximum resolution of the instrument is ≈ 0.2 nm. Deposition of particles onto Formwar-coated copper grids was performed using highly diluted suspensions of freshly prepared and 6-year-old magnetite. The average size distribution was determined by evaluating 200 particles using the UTHSCSA Image Tool 2.00 software.

The *specific surface area* (a^s_{BET} given in unit m^2/g) of freeze-dried solid samples was determined from the BET analysis of nitrogen adsorption isotherm measured at 77 K over the range 0–0.95 of relative pressure (p/p_0) using a Micrometrics Gemini II 2375 surface area analyzer.

Potentiometric Acid-Base Titrations. – The pH-dependent surface charge was determined by potentiometric acid-base titration under a CO_2-free atmosphere. An indifferent electrolyte (NaCl) was used to maintain constant ionic strength, ranging between 0.01 and 1 mol dm^{-3}. Before titration, the suspensions or solutions were stirred and bubbled by purified nitrogen for 15 min. Equilibrium titration was performed in a self-developed titration system (GIMET1) consisting of two Dosimat 665 burettes (Metrohm), a nitrogen bubbler, a magnetic stirrer and a high performance potentiometer. The course of titration (amount and frequency of the titrant, bubbling, stirring, millivolt measurements) was controlled by an IBM PS/1 computer using AUTOTITR software. The pH-measuring Radelkis OP-0808P (Hungary) combination glass electrode was calibrated using three buffer solutions (Radelkis, Hungary) to check the Nernstian response. Evaluation of titration data was based on the calculation of the material balance for H^+/OH^- ions. The measuring system had to be calibrated for the H^+/OH^- ion concentration, which in turn was put into the material balance equations. The experimental activity coefficients of H^+/OH^- ions were determined from the background electrolyte titration at each ionic strength. The H^+/OH^- concentration was calculated knowing the concentration of acid and base titrants, the volume of portions and the dilutions, and their activities were calculated from the measured pH and the ionization constant of water. If the response of the glass electrode is perfect, the activity *vs.* concentration plots give straight lines, and their slopes provide the values of experimental activity coefficients at different electrolyte concentrations.

The net proton surface excess amount ($\Delta n^s = n^s_{H^+} - n^s_{OH^-}$) is defined as the difference between H^+ ($n^s_{H^+}$) and OH^- ($n^s_{OH^-}$) surface excess amounts related to the unit mass of solid. The surface excess amount of a solute i (Γ_i) can be determined[2] experimentally from the initial ($c_{i,0}$) and the equilibrium concentration ($c_{i,e}$) of the solute ($n^s_i = V(c_{i,0} - c_{i,e})/m$, where V is the liquid phase volume and m is the mass of the adsorbent; $\Gamma_i = n^s_i/a^s$, where a^s is the specific surface area of the adsorbent, for adsorption from dilute solutions. The values of excess $n^s_{H^+}$ or $n^s_{OH^-}$ were calculated at each point of titration from the initial and the equilibrium concentrations of the H^+ and OH^- ions using the actual experimental activity coefficients from the corresponding background electrolyte titration.

Since this method is based on determination of the change in the H^+/OH^- concentration in the liquid phase due to interfacial protolytic processes, any acid/base impurities of the titrated sample and its dissolution at extreme pHs will interfere with the surface charge density, as showed for alumina[18] before, and so careful sample preparation is required. In the case of magnetite, the stock suspension was stored in 0.001 mol dm^{-3} HCl, so its medium contained excess H^+ ions. Therefore, the equilibrium supernatant obtained by centrifugation at 13000 RPM for 2 hours was also titrated in parallel with suspensions, and its consumption was subtracted from the suspension consumption. The different NaCl concentrations in suspensions and solutions were adjusted by adding calculated amounts of NaCl stock solutions.

Electrophoretic Mobility Measurement. – Electrophoretic mobilities of the fresh and aged samples were measured at 25 ± 0.1 °C in a disposable zeta cell (DTS 1060) of a NanoZS (Malvern, UK) apparatus. To obtain optimal conditions for measurements, the intensity of scattered light had to be at a medium level (≈ 10^5 counts per second). Therefore, the dilution series of pure magnetite sol were tested prior to detailed studies of the effects of pH and electrolyte addition on the electrophoretic mobility of iron oxide nanoparticles. According to this preliminary measurement, the optimal condition was reached at a 0.1 g/L magnetite content. The pH was adjusted in the range of about 3 to 10 by HCl or NaOH solutions, and after waiting for an hour to reach equilibrium, it was measured directly before introducing the samples into the zeta cell. The pH-dependence of electrophoretic mobilities at 0.001, 0.01 and 0.1 mol dm^{-3} NaCl was determined.

Dynamic Light Scattering (DLS) Measurements. – These measurements were performed using a NanoZS apparatus (Malvern, UK) with the laser beam λ = 633 nm produced by a He-Ne laser, operating in back-scattering mode at an angle of 173°. The same measuring cell (DTS 1060) was also used for the size determination studies. Freshly pre-

pared and aged magnetite particles from the stock suspension were dispersed in electrolyte solutions to get a 0.1 g/L solid content. The pH of the systems was adjusted in the range from 3 to 10, and was measured directly before a sample was placed into the cell. The pH-dependent particle aggregation was measured in 0.001, 0.01 and 0.1 mol dm^{-3} NaCl solutions.

The correlation functions were evaluated by third- order cumulant analysis. The first-order autocorrelation function, $g^1(\tau)$, was given as $g^1(\tau) = \exp(-\mu_1\tau+(\mu_2/2!)\tau^2+(\mu_3/3!)\tau^3+...)$, where μ_1 is an average decay rate; μ_1 characterizes the mean, μ_2 the width and μ_3 the skewness of the distribution. If translational diffusion is the dominant dynamics ($\boldsymbol{q}r_h << 1$), the diffusion coefficient (D_t) can be calculated, $\mu_1 = D_t\boldsymbol{q}^2$, where the scattering vector ($\boldsymbol{q}$) is $\boldsymbol{q} = (4\pi n/\lambda)\sin(\Theta/2)$, and n is the refractive index of the medium, λ is the laser wavelength, Θ is the scattering angle, k is the Boltzmann constant, T is the temperature and η is the viscosity of the medium. From the Stokes-Einstein equation ($r_h = kT/6\pi\eta D_t$), the hydrodynamic radius (r_h) can be obtained.

To get comparable results, all samples had to be measured under the same experimental conditions. Therefore, the same preparation method was applied for each sample, and the kinetic stage starting from a short ultrasonic treatment was detected. The Z average size values calculated from 3rd order cumulant fits of the measured correlation functions at a given kinetic stage (measured 50 seconds after ultrasonication) are presented.

RESULTS AND DISCUSSION

XRD Identification of Iron Oxides Phases

The crystalline phase transformation of magnetite samples during long storage was studied by the XRD method. We should note that our synthetic products retained dark, black to brownish colour and strong magnetism, which are distinctive properties of magnetic iron oxides (magnetite and maghemite) even after storage for 6 years. The XRD patterns of freeze-dried iron oxide samples of different ages are given in Figure 1. The appearance of characteristic peaks with various intensities can be seen in each case. The diffractograms clearly show a significant difference between the crystalline phases of freshly prepared and aged samples. The XRD patterns were evaluated using the Bragg equation to determine the *d*-spacings and *hkl*-indices belonging to the most intensive diffraction peaks. The *d* values calculated from the position of diffraction peaks and the corresponding Miller indices define clearly the crystalline phases present in the samples. The presence of magnetic iron oxides, such as magnetite (Fe_3O_4) and maghemite (γ-Fe_2O_3), was supposed owning to the definite magnetic features of the samples even after 6-year-storage. It should be noted that the diffraction pattern of magnetite and maghemite is almost the same due to their analogous inverse cubic spinel crystal structure. The small difference between their lattice parameters, 0.839 nm and 0.835 nm, respectively, results in a slight shift of all peaks of maghemite to higher 2Θ values as compared to those of magnetite.[8,19] Hence, identification of coexisting magnetite and maghemite phases is difficult due to the overlapping peaks. However, some typical peaks can be found in the JCPDS database, which preferably correspond to the magnetite (at 35.6°, 42.3°, 57.4°, and 63.1°) or rather maghemite phase (at 31.8° and 49.2°). Since peaks appearing at 35.6 and 42.3 2Θ degrees are attributed to the Fe_3O_4 phase considering the *d* values and Miller indices, its presence can be proved by the XRD patterns. The analysis based on the JCPDS database clearly showed that the magnetite phase is present in all three samples, as indicated in Figure 1.

It can be seen that the intensities of the above mentioned characteristic peaks at 35.6° and 42.3° decrease gradually with time, which probably indicates a decrease in magnetite content with increasing storage time. In contrast to fresh magnetite, new, sharp peaks appear in

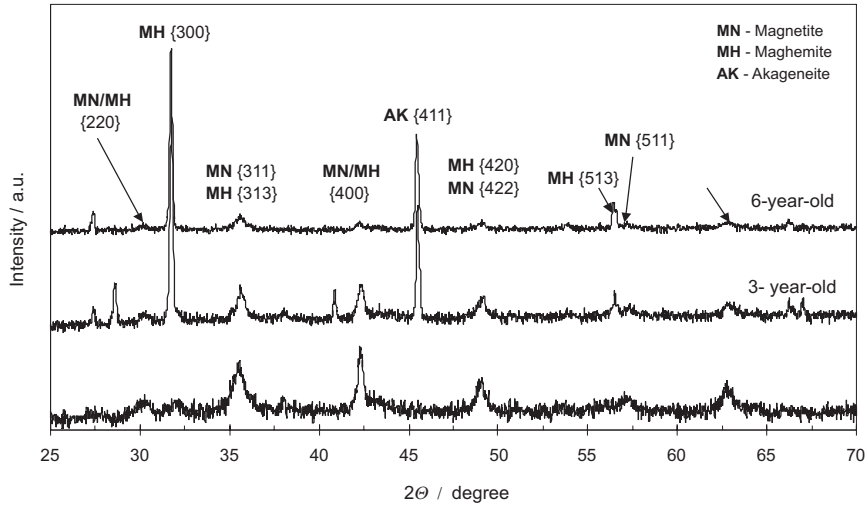

Figure 1. XRD patterns of freshly prepared and aged (3- and 6-year-old) magnetite samples.

TABLE I. Spontaneous coarsening of magnetite nanoparticles with time (Ostwald ripening)

Methods	XRD (Scherrer)	TEM (200 particles averaged)		N_2 adsorption at 77 K
Storage	size / nm	size / nm	Std. Dev.	a^s (BET) / $m^2\ g^{-1}$
no, fresh	12.84	6.69	1.72	95.35
3 year	17.76	–	–	28.37
6 year	20.35	8.05	1.82	27.29

the XRD patterns of older iron oxide samples at 31.8° and 45.5°, which correspond to maghemite (γ-Fe_2O_3) and akageneite (β-FeOOH) major phases, respectively. Further analysis of diffractograms reveals several minor crystalline phases of iron oxihydroxides (hematite, goethite, lepidocrocite, *etc.*) in addition to major magnetite, maghemite, akageneite phases. A brief summary of spontaneous transformations, *i.e.,* interconversions among the different major iron oxides has been published in the literature.[8] Maghemite and/or hematite formation from magnetite through the oxidation process in solid samples under atmospheric conditions has been proved;[8,19] however, a detailed study of possible transformations has not been done yet. In solid state, hematite forms from magnetite at higher temperatures (370–600 °C), and its transformation to maghemite takes place over years even at room temperature.[20] The latter was accelerated effectively by aeration oxidization of acidified aqueous suspension of magnetite nanoparticles at about 100 °C for an hour, as published recently.[12] Oxidation kinetics of aqueous colloidal 9-nm magnetite nanocrystals was studied[21] in the alkaline region at different temperatures, 24, 50, 65 and 80 °C. It was proved that the transformation of magnetite to maghemite is a topotactic reaction, in which the original particle morphology is maintained throughout. Besides the sensitivity of the magnetite phase to aerobe conditions, enhanced dissolution of nanoparticles, dissolved species and their recrystallization in aqueous systems have to be taken into consideration. Higher solubility of smaller particles may lead to their transformation to larger ones via solution, followed by precipitation on the surface of larger particles, a process called Ostwald ripening. In our case, the maghemite formation can be assigned to slow oxidation, since the aqueous magnetite suspension was not stored under anaerobe conditions. However, the formation of akageneite was also proved by XRD measurements. This kind of iron oxide forms by the hydrolysis of $FeCl_3$ and is stable in acidic suspensions.[22] Liu *et al.*[23] studied the phase transformation from $Fe(OH)_3$ gel to α-Fe_2O_3 particles and akageneite (β-FeOOH) was obtained as an intermediate product formed by the dissolution/reprecipitation mechanism at pH < 4.5 in the presence of Cl^- ions. Cl^- ions probably diffuse into the Fe^{III} polymer at low pH because of the affinity between Fe^{III} ions and Cl^- ions, and influence both nucleation and growth of crystals, thus resulting in the formation of the intermediate product akaganeite. Since enhanced dissolution of magnetite nanoparticles of ≈ 12 nm (similar to ours) produces 0.0005 mol dm^{-3} Fe^{III} ions dissolved in aqueous medium at pH ≈ 3 over weeks,[11] it can be supposed that the magnetite nanoparticles stored in 0.001 mol dm^{-3} HCl solution dissolve slowly releasing Fe^{III} ions at pH ≈ 3, which interact with Cl^- ions present as counterions around the positively charged particles, and the formed polymer species adsorb on the larger particles initiating the growth of an akageneite layer on the surface of magnetite/maghemite crystals. It seems that the amount of akageneite crystalline phase formed during the first 3-year-storage slightly decreases in the second storage period, since the intensity of the sharp peak at 45.5°, assigned to akageneite crystals, declines somewhat compared to the XRD patterns of 3- and 6-year-old samples in Figure 1. The assumed formation of an akageneite shell on the magnetite/maghemite core is also supported by further evaluation of XRD results and a TEM study of particle size.

The average size of iron oxide particles can be estimated from the broadening of the most intensive peak of the XRD pattern by using the Scherrer equation. The particle size values were determined from the peak at 42.3 degrees of 2Θ as the most intense one according to the JCPDS database. The calculated values are given in Table I. The data clearly show that a significant increase in the average size of crystallites took place during the long storage time.

Characterization of Particle Morphology and Size Distribution

TEM images of fresh and aged magnetite samples are shown in Figure 2. The non-uniform size distribution of particles is obvious. Rounded crystals are observable in both cases, which is in good accord with the previously found[12,14] general feature of synthetic magnetite samples. Maghemite crystals always adopt the shape of their precursor; therefore, they cannot be identified on the basis of morphology. Akageneite exhibits different shapes (spindles and rods) with generally narrow size distributions;[8] however, this was not observed anywhere in the

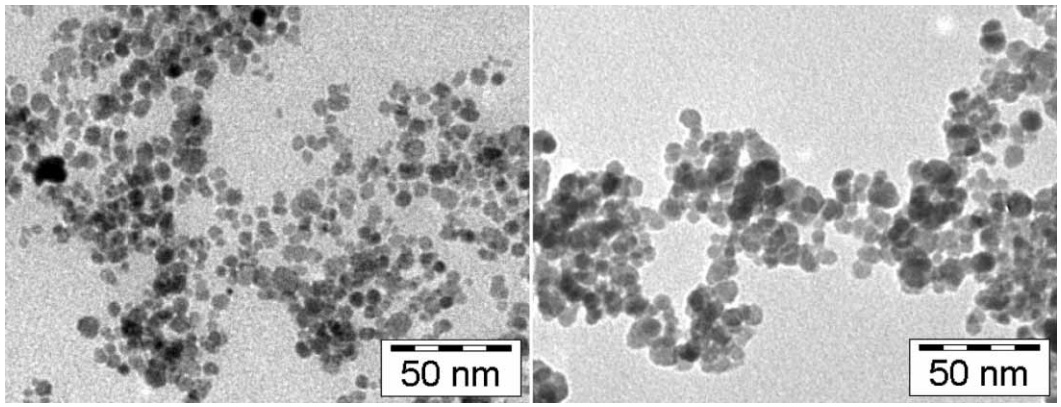

Figure 2. TEM image of a freshly prepared (left) and a 6-year-old (right) magnetite sample.

TEM images of the 6-year sample. This is perhaps due to its very small amount, which is slightly inconsistent with the definite presence of akageneite crystalline phase proved by the XRD patterns of aged samples (Figure 1). A more acceptable reason for hiding individual akageneite crystals is that akageneite forms as a shell on the magnetite/maghemite core.

The exact size of iron oxide nanoparticles cannot be determined because of the slight polydispersity of samples. Size distributions of fresh and aged magnetite samples can be compared in Figure 3. It can be seen that the particle size falls in the same range, but the characteristic value becomes slightly greater with time. The average sizes estimated by calculating 200 particles are 6.7 ± 1.7 nm for the freshly prepared and 8.1 ± 1.8 nm for the 6-year-old samples (Table I). These values are smaller than those determined from the XRD peak broadening. There are various reasons for systematic differences observed in the particle size determined by TEM and XRD methods, such as (i) the field of view is relatively small and randomly chosen by the analyst, raising the possibility that the region analyzed by TEM may not be characteristic of the whole sample, and (ii) both the baseline and the half width of the XRD peak cannot be determined precisely due to the relatively high noise, causing inaccuracy in the calculated particle sizes.

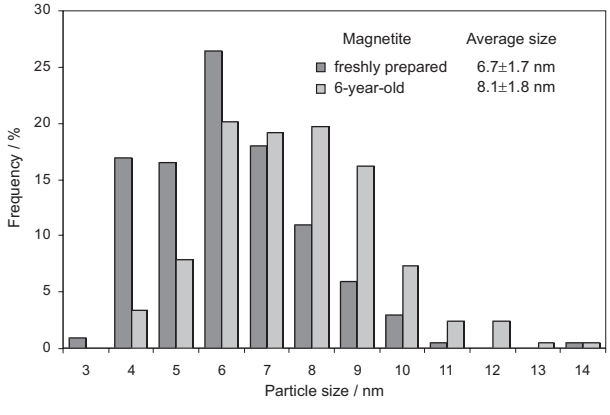

Figure 3. Size distribution of fresh and aged magnetite samples determined by TEM analysis.

Specific Surface Area Determination

The specific surface areas (a^s_{BET}) of the iron oxide samples determined by nitrogen adsorption at 77 K are summarized in Table I. These values of fresh and aged magnetites fall in the range usually published in the literature[8] (4–130 m^2/g). The specific surface area of the fresh magnetite sample was quite high (≈ 95 m^2/g), then a significant decrease to ≈ 28 m^2/g occurred during storage for 3 years (Table I). No or only a very small change followed in the following 3 years, the difference between the 3-year- and the 6-year-old samples being within the accuracy of this measurement. The specific surface area of magnetite[8] obtained by precipitation was about 100 m^2/g, which is in good agreement with the a^s value of our freshly prepared sample (≈ 95 m^2/g). Since the specific surface area of pure maghemite originating from magnetite is close to that of its precursor,[8] the significant decrease observed here should be explained by other processes taking place during recrystallization of Fe_3O_4 on the particle surface. Coalescence of individual nanocrystals is highly probable during recrystallization in aqueous medium, so less space remains accessible to nitrogen molecules on the surface of particles. The decrease in the specific surface area of aged samples is in good accord with their larger particle size obtained from the TEM and the XRD analysis.

The low-temperature N_2 adsorption isotherms showed that all samples are practically non-porous materials. But, a small hysteresis loop appears between the adsorption and desorption curves indicating very low porosity of each iron oxide, which cannot be explained by their solid phase properties, since magnetite, maghemite originating from Fe_3O_4 and akagenite are non-porous materials according to the literature.[8] This cannot even be assigned to the presence of narrow tunnels in the akageneite structure,

since these are not accessible to nitrogen molecules because of the size limitation. It can be supposed that the curved surfaces between the stuck nanoparticles (6–9 nm) save place for the capillary condensation of nitrogen at 77 K, resulting in a hysteresis loop measured over the mesopore range (2–50 nm), since these curvatures fall in the lower region of mesopores. The 6-year-old sample showed a smaller hysteresis loop than the 3-year-old one in line with a slight decrease in the specific surface area (Table I), which might indicate the increase in particle size during long storage.

pH-Dependent Surface Charging

Significant changes, obvious effects of ageing on the solid phase and on the solid/gas interfacial properties were determined. These were the consequence of slow processes taking place in the aqueous magnetite dispersion for years. There is a substantial difference between the dry and wet surface chemistry, especially for metal oxides dispersed in water, as noted in the introduction of the outstanding book by Kosmulski.[24] Now the question is how ageing is expressed directly through changes in the aqueous interfacial properties of magnetite nanoparticles.

In an aqueous medium, pH and ionic strength dependent charges develop on amphoteric surface hydroxyls (Fe-OH). The following protonation and deprotonation reactions can take place on the surface of iron oxide particles:

$$\underline{\text{Fe}}\text{-OH} + \text{H}^+ \leftrightarrow \underline{\text{Fe}}\text{-OH}_2^+ \quad (1)$$

$$\underline{\text{Fe}}\text{-OH} \leftrightarrow \underline{\text{Fe}}\text{-O}^- + \text{H}^+ \quad \text{or}$$
$$\underline{\text{Fe}}\text{-OH} + \text{OH}^- \leftrightarrow \underline{\text{Fe}}\text{-O}^- + \text{H}_2\text{O} \quad (2)$$

According to the IUPAC recommendation,[25] H^+ and OH^- ions are considered to be the potential-determining ions. When surface charge development occurs by direct proton transfer from the aqueous phase, the surface charge density ($\sigma_{0,H}$) and surface potential (ψ_0) can be defined analogously to the Nernstian surfaces:

$$\sigma_{0,\text{H}} = F(\Gamma_{\text{H}^+} - \Gamma_{\text{OH}^-}) \quad (3)$$

$$\psi_0 = (RT/F)\ \ln[\text{H}^+]/[\text{H}^+]_{\text{pzc}} = (RT/F)2.3(\text{pH}_{\text{pzc}} - \text{pH}) \quad (4)$$

where Γ_i is the surface excess concentration of species i, R is the gas constant, T is the temperature and F is the Faraday constant. Direct measurement of surface potential using an electrode made of a hematite crystal, called the single-crystal metal oxide electrode (SCrE), was invented and discussed from both theoretical and practical points of view by Kallay *et al.*[26] A further study of the hysteresis and equilibrium at the aqueous interface of hematite was published recently.[27] Surface potential was measured as a function of pH in different electrolyte solutions and the slope of these curves was found to be lower than the Nernstian, especially in the basic region. It was thus concluded that the surface potential of hematite does not obey the Nernst equation given above. Theoretical analysis based on the surface complexation models (SCMs) resulted in equations, *e.g.*, the surface potential associated with separate protonation and deprotonation processes is equal to:

$$\psi_0 = (RT\ \ln 10/F)\ (\text{pH}_{\text{pzp}} - \text{pH}) - (RT/2F)\ \ln\ (\Gamma_{\equiv\text{OH}_2^+}/\Gamma_{\equiv\text{O}^-}) \quad (5)$$

where the first term is the Nernstian, the second is responsible for the decrease in the magnitude of surface potential, *i.e.,* the lowering of the slope of the ψ_0 (pH) function.[26] It should be noted that $\Gamma_{\text{H}^+} = \Gamma_{\equiv\text{OH}_2^+}$ and $\Gamma_{\text{OH}^-} = \Gamma_{\equiv\text{O}^-}$, and the point of zero potential (pzp), *i.e.*, the pH_{pzp} value at which $\psi_0 = 0$, must be equal to the pH of the point of zero charge (pH_{pzc}), *i.e.*, the pH_{pzc} value at which $\sigma_0 = 0$, in the presence of indifferent electrolytes.

The pH-dependent surface charge density is experimentally accessible from potentiometric acid-base titration of oxide suspensions.[24,28,*etc.*] The net proton surface excess amount ($\Delta n^{\text{s}} = n^{\text{s}}_{\text{H}^+} - n^{\text{s}}_{\text{OH}^-}$ given in mmol/g) can be directly calculated at each point of titration from the material balance of H^+/OH^- and the mass of oxide sample titrated, if no other acid or base consuming reactions take place during titration. The net proton surface excess ($\Delta\Gamma_{\text{H,OH}} = \Gamma_{\text{H}^+} - \Gamma_{\text{OH}^-}$ given in mmol/m^2) can be calculated if the specific surface area (a^{s}) of oxide sample is known, since $\Gamma_i = n_i^{\text{s}}/a^{\text{s}}$. The $\sigma_{0,\text{H}}$ (or $\Delta\Gamma_{\text{H,OH}} = \Gamma_{\text{H}^+} - \Gamma_{\text{OH}^-}$) *vs.* pH curves, the so-called charge-potential functions, were determined at several concentrations of an indifferent electrolyte intersect at a common pH. This is called a common intersection point (cip).[4,25] In the absence of specifically adsorbed ions, the cip coincides with the $\sigma_{0,\text{H}} = 0$ surface charge (where the $\Gamma_{\text{H}^+} = \Gamma_{\text{OH}^-}$); this particular pH is referred to as the point of zero charge (pzc). The pH of pzc is characteristic of each metal oxide in an aqueous medium. Several experimental data of pzc for iron oxides are available in the literature, the values being between 3.8 and 9.9 for magnetite.[8,11,24,29]

Characterization of the change in the pH-dependent surface charging of magnetite during longer storage is of great practical importance in terms of application of water-based magnetic fluids. The net proton surface excess of a freshly prepared and a 6-year-aged sample was determined by potentiometric acid-base titration over the pH range 3 to 11 at different ionic strengths. Evaluation of the experimental data from acid-base titration of amphoteric solid material demands cautious work. The different approaches are accepted in the literature and summarized perhaps in the most comprehensive way in the book of Kosmulski.[24] As regards solution chemistry,

the experimental data of colloid titration are significantly less accurate and reproducible than those in homogeneous systems. The situation at the electrified interface is more complicated. Other acid or base consuming reactions (*e.g.,* the presence of acid/base impurities, dissolution of the solid at lower or higher pHs) can take place in parallel with the surface charging processes, which cannot be separated experimentally, as analyzed in Ref. 30. However, excluding all this, the net proton surface excess amount related to the unit mass of the solid can be calculated directly and plotted as a function of pH. In the case of magnetite, since the stock suspension was stored in 0.001 mol dm^{-3} HCl, both the surface and the medium contained excess H^+ ions in an exactly unknown amount. The double calibration of our titration system for both the pH and the H^+/OH^- concentration allowed us to correct the measured net proton consumption of magnetite suspension. On the one hand, the H^+ concentration of the equilibrium supernatant was measured and proved to be independent of NaCl concentration over the range of pH = 3 to 9, so its additive correction became possible. On the other hand, the surface excess H^+ concentration in the initial state at pH ≈ 3 and 0.001 mol dm^{-3} ionic strength was estimated and subtracted from the calculated material balance of H^+/OH^- ions during titration.

The pH-dependence of the net proton surface excess amount (Δn^s) of magnetite can be seen in Figure 4. The reversibility of forward and backward titration was excellent. Below pH ≈ 4 and above pH ≈ 10, dissolution of the amphoteric solid may occur, and therefore in aqueous media the solubility of a solid material is worth considering. This process is influenced not only by the pH, temperature and ionic strength of the system, but also by the particle size and crystal defects in the oxide.[8] In general, the solubility of Fe^{III} oxides is low and Fe^{II} oxides are sparingly soluble. This means that, except for extreme pH values, these compounds maintain a very low (lower than 10^{-6} mol dm^{-3}) level of total Fe in solution in the absence of complexing or reducing agents. Magnetite usually dissolves faster than pure Fe^{III} oxides due to its Fe^{II} content and also because Fe^{III} occurs in octahedral and tetrahedral sites. However, the activity of dissolved Fe^{III} species remains below ≈10^{-5} mol dm^{-3}, between pH ≈ 4 and ≈10.[8] Hence, dissolution of magnetite can be neglected in the studied pH range. The magnetite pzc seems to be at pH = 7.9 ± 0.1 and this value falls in the range given in the literature.[8,24,29] Substantial simplifications and several hypotheses relating to treating surface charge formation are known and the problems of modeling the surface charging of oxides have been discussed in several papers.[24,31,*etc.*] The pH- and ionic strength-dependent surface charge formation process can be described by various model approximations, the site-binding electrostatic or surface complexation models (SCMs) models being the most widely accepted.[3,24,28,31,32,*etc.*] A good comparison of 1pK and 2pK models is given by Borkovec[33] and the relationship of equilibrium parameters has been clarified by Kallay's school.[34] The surface charge development may be affected by the solubility of the solid, which is not incorporated in the models. The following reactions represent the charge formation on the magnetite surface:

$$\underline{\text{Fe}}\text{-OH} + \text{H}^+ \leftrightarrow \underline{\text{Fe}}\text{-OH}_2^+ \quad K_{\text{a,1}}^{\text{int}} = \frac{(\underline{\text{Fe}} - \text{OH}_2^+)}{(\underline{\text{Fe}} - \text{OH})(\text{H}^+)_\text{s}} \tag{6}$$

$$\underline{\text{Fe}}\text{-OH} \leftrightarrow \underline{\text{Fe}}\text{-O}^- + \text{H}^+ \quad K_{\text{a,2}}^{\text{int}} = \frac{(\underline{\text{Fe}} - \text{O}^-)(\text{H}^+)_\text{s}}{(\underline{\text{Fe}} - \text{OH})} \tag{7}$$

where $K_{\text{a,1}}^{\text{int}}$ and $K_{\text{a,2}}^{\text{int}}$ are the invariant intrinsic equilibrium constants; the brackets mean the activity of the species. The surface species $\underline{\text{Fe}}$-OH, $\underline{\text{Fe}}$-OH_2^+ and $\underline{\text{Fe}}$-O^- are assumed to have activity coefficients equal to unity. The activity of surface protons $(H^+)_s$ is corrected for the energy expended in moving them from the bulk phase (infinite distance from the surface) to the charged surface (at distance zero), where the reaction occurs. $(H^+)_s$ can be expressed in terms of the bulk solution hydrogen ion activity, (H^+):

$$(\text{H}^+)_\text{s} = (\text{H}^+)\exp\left(\frac{e\Psi_0}{kT}\right) \tag{8}$$

where $e\Psi_0$ is the electric potential energy (e is the electron charge), and kT is the thermal, kinetic energy (k is the Boltzmann constant, T is the temperature).

The intrinsic equilibrium constants were calculated for magnetite. The experimental data of titration were evaluated using the numerical data-fitting program FITEQL.[35] The choice of different surface complexation models (constant capacitance (CC), diffuse layer (DL), Stern and triple layer (TL)) is optional. The measured data of magnetite titration might be well fitted by choosing any SC model. An example of the quality of the fitting of curves optimized by FITEQL using the CC approach and the experimental points calculated on the basis of material balance of added H^+/OH^- is shown in Figure 4. The calculated equilibrium constants were log $K_{\text{a,1}}^{\text{int}}$ = 6.6±0.1, log $K_{\text{a,2}}^{\text{int}}$ = –9.1±0.1. The pH of the pzc was calculated according to the relation[8,25] pzc = 0.5 (log $K_{\text{a,1}}^{\text{int}}$ – log $K_{\text{a,2}}^{\text{int}}$), and this value ($pH_{pzc,calc}$ = 7.9±0.2) correlates well with the observed pzc (pH_{pzc} = 7.9±0.1). Only a few studies addressing the surface ionization of synthetic magnetite can be found in the literature.[36,37] Log $K_{\text{a,1}}^{\text{int}}$ = 4.4 for protonation of $\underline{\text{Fe}}$-OH sites and log $K_{\text{a,2}}^{\text{int}}$ = 9.0 for protonation of $\underline{\text{Fe}}$-O^- sites on magnetite surface have been reported. These values agree more or less well with our model calculation. It should be noted

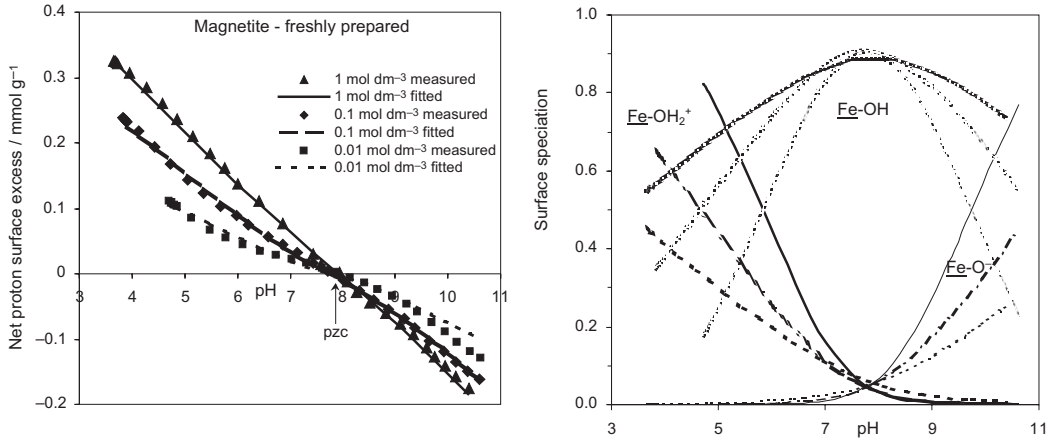

Figure 4. Net proton surface excess amount of magnetite as a function of pH at different NaCl concentrations (left). The points were calculated from the material balance of H^+/OH^- in the course of equilibrium acid-base titration. The continuous lines were numerically fitted using FITEQL[35] (constant capacity model, $C = 1.6$ F/m^2). The calculated equilibrium constants are $\log K^{int}_{a,1} = 6.6\pm0.1$ and $\log K^{int}_{a,2} = -9.1\pm0.1$. The pH-dependent distribution of surface species (right).

that the experimental conditions and the quality of magnetite samples in these papers were different from ours, and so different variables (specific surface area, ionic strength, *etc.*) were used, which also influenced the calculated log K values.

The number of positively or negatively charged surface sites increases with increasing ionic strength due to the charge screening effect of the electrolyte,[28] as shown in Figure 4 (right) where calculated data are plotted in the function of pH.

The net proton surface excess of the magnetite sample aged in aqueous suspension for 6 years was determined and evaluated in the same way as described above for the freshly prepared magnetite. The measured data of fresh and aged magnetites are compared in Figure 5. The overall features of the pH-dependent surface charge formation on magnetite and akageneite coated magnetite/maghemite are the same. However, significant differences between the fresh and aged samples can be clearly seen on the left hand side of Figure 5, such as (i) the shift of pzc from ≈8 to ≈7 and (ii) a significant (about one third) decrease in the net surface proton excess compared to unit mass of iron oxides, in good accord with the decrease in specific surface area during storage for 6 years (Table I). Calculating the surface charge *vs.* potential curves (on the right hand side of Figure 5) as it is usually done in the literature,[4,24] the shift of pzc from ≈8 to ≈7 remains the same; however, only a minimal difference in surface charge density can be seen in the acidic region, the curves of fresh and aged samples at different salt concentrations run practically parallel. It can be stated that the charge-potential curves conceal somewhat the essence of differences in systems like the present one,

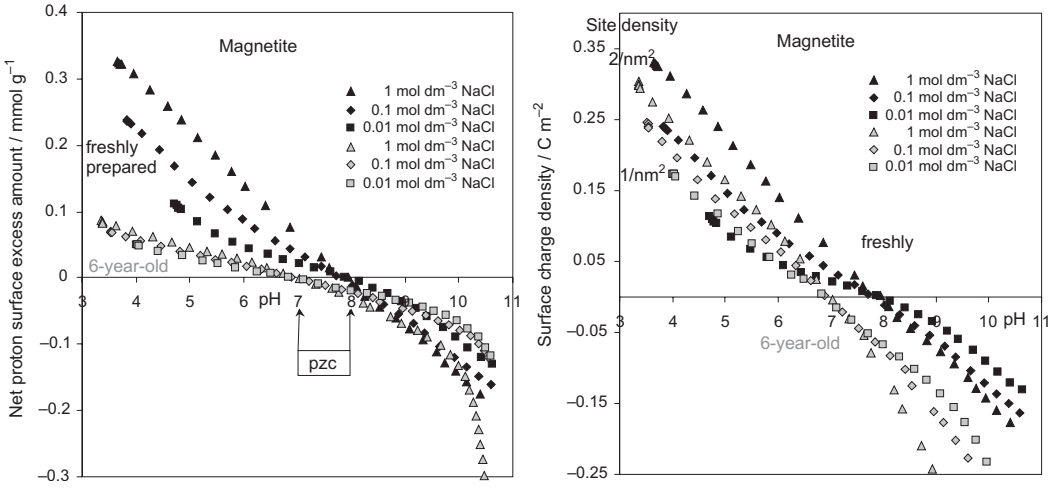

Figure 5. The pH-dependent surface charging: a comparison between the freshly prepared magnetite and the aged sample stored in an aqueous suspension at pH ≈ 3 in refrigerator for 6 years. The net proton surface excess amount ($\Delta n^s = n^s_{H^+} - n^s_{OH^-}$ given in mmol/g) was calculated directly.

where the inherent changes were related to the ageing of magnetite nanoparticles. As regards the surface charge density range (0.17–0.31 C/m^2) reached at pH ≈ 4 in Figure 5 (right), it is about two times greater than that of coarse (0.22 μm) magnetite (≈ 0.08–0.17 C/m^2) published before.[36,37] However, the calculated amount of the active site (≈1–2 per nm^2) on the magnetite surface for proton binding is less than half of that (5.2 site/nm^2) calculated for a fine (≈12 nm) magnetite.[11] We should note that this kind of literature data are often not trustworthy.

The pzc of the aged sample at pH ≈ 7 agrees quite well with the iep (isoelectric point) and pzc data of akageneite published mostly at pH = 7.2 in the literature.[24] It seems that the aqueous interfacial property of aged nanoparticles is rather similar to that of akageneite. This supports entirely the assumption of the akageneite shell formation on magnetite/maghemite core discussed above. The behaviour of aged sample in the alkaline region is somewhat different from that expected for the surface charging of oxides *via* deprotonation reaction (Fe-OH + $OH^- \leftrightarrow$ Fe-O^- + H_2O) like in the case of the fresh magnetite sample, where the dissolution of solid phase was neglected. Since the solubility of akageneite is much higher than that of magnetite in alkaline media,[8] the akageneite shell can dissolve during titration, especially above pH ≈ 10 consuming a large OH^- amount, which causes a sharp decrease in the net proton surface excess amount (left hand side of Figure 5) calculated from the material balance of H^+/OH^- at each point of titration according to our evaluation method. The dissolution of akageneite shell in alkaline region is supported by the fact that the forward and backward titration curves were not reversible above pH ≈ 9.5 (not shown here). The lack of reversibility and the probable dissolution of solid phase preclude the application of surface complexation modelling without taking into account dissolution reactions and acid-base reactions of the dissolved species. The latter could be done for alumina,[18] since all the equilibrium data were available in the literature. The present knowledge on akageneite is far from this expectation.

Charge State of Particles in Electrolyte Solutions

Electrokinetic measurements provide independent information on the electric double layer of charged particles. The measured electrophoretic mobility can be converted to electrokinetic (zeta) potential on the well-known theoretical basis with several assumptions, limitations[38] and criticisms, as mentioned in a recent paper.[39] The sign of these electrokinetic data is the same as that of the excess charge of a particle moving together with the adhered layer of counterions, and its magnitude is somewhat proportional to the particle charge. The sign of the electrophoretic mobility measured in the metal oxide dispersions reverses at a characteristic pH, where these amphoteric particles do not hold excess charge. It can be identified as the pH of the isoelectric point (iep). This is the only model-independent quantity from electrokinetic measurements.[31]

The pH dependence of electrophoretic mobilities for fresh and 6-year-old magnetite particles was measured at different ionic strengths. As shown in Figure 6, the electrophoretic mobility of magnetite particles decreases significantly over the whole range of pH at each NaCl concentration. The symmetric shape of the mobility-pH plot near the iep indicates the significance of the H^+/OH^- ions in determining surface charging. While the ionic strength dependence of surface charging curves (Figure 5) showed the usual opening shape, indicating the effective charge screening of indifferent electrolyte,[4,24,25,28] the electrophoretic mobility *vs.* pH curves ran together, especially in the case of the fresh sample, and seemed to disobey the trend expected with changing ionic strength.[38] We suppose a specific behavior of nanoparticles in the electric field, since their size (< 10 nm, see Table I) is commensurable with the thickness of the diffuse layer around them, as given by the Debye length between ≈10 and 1 nm in 0.001 to 0.1 mol dm^{-3} 1:1 electrolyte in which the measurements were performed. These nanoparticles should move together with the accompanying counterions, but the deformation of their local electric field is questionable, and there is no doubt that the concept of slipping plane failed in the world of nanoparticles. In principle, the Hückel approach can be applied to convert the mobility values to electrokinetic (zeta) potential, but it was not worth calculating. Data showing the common ionic strength dependence of micron sized synthetic or commercial magnetite have been published[11,36] but no reliable electrokinetic data for magnetite nanoparticles are available in the literature.

Apart from the unusual ionic strength dependence, the pH where the sign of electrophoretic mobility reverses can be identified at pH ≈ 8 and pH ≈ 7 as pH_{iep} for the fresh and the aged magnetite sample, respectively. These pH_{iep} values are in quite good agreement with the pH_{pzc} determined from the surface charge titration curves, as shown in Figure 5. The fact that the pH_{iep} values of both magnetite samples coincide with the pH_{pzc} indicates that the electrolyte NaCl applied here may be indifferent, so Na^+ and Cl^- ions obey only the electrostatic constraint. The 1-pH unit shift in pH_{iep} supports the assumption discussed above of the existence of an akageneite layer on the magnetite/maghemite core in the sample aged for 6 years.

pH-Dependent Aggregation of Nanoparticles in Electrolyte Solutions

The studied magnetite suspensions are electrostatically stabilized from the point of view of colloidal stability. Particles either aggregate or disperse, depending on the structure of the local electric field formed on particle surfaces. Aggregation processes in dilute suspensions

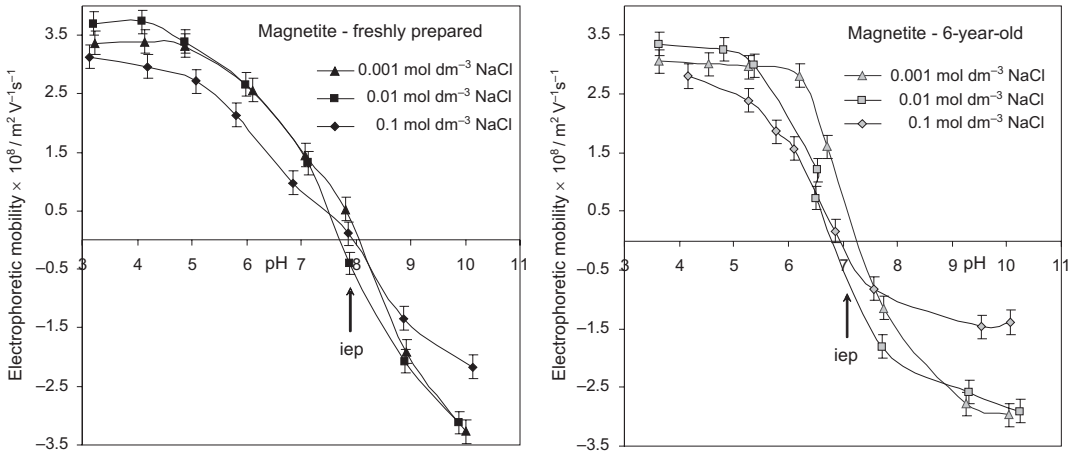

Figure 6. The pH-dependent charge state of fresh and aged magnetite nanoparticles.

can be characterized by particle size determination. Dynamic light scattering (DLS) can provide reliable size data even when the system is undergoing coagulation.[40]

The pH-dependence of the hydrodynamic size calculated from the cumulant analysis of first-order correlation functions is shown in Figure 7. It is obvious that the pH induced particle aggregation is surprisingly different for the fresh and aged samples at each NaCl concentration. The colloidal stability of charged particles is actually determined by their surface charge state. The fresh sample shows a significant increase in average particle size over the range of pH ≈ 7–9 at the lowest salt concentration, proving a pronounced aggregation near the pH of pzc where the electrostatic repulsion between particles is negligible and particles generally undergo fast coagulation, in accordance with the literature.[28,41–44] We did not experience any unusual behavior regarding the colloidal stability of ≈10-nm magnetite particles as predicted for the smallest (1–3 nm) hematite nanoparticles.[45] The pH range of aggregation becomes broader at higher salt contents. The absolute aggregation rate constants for pH-dependent aggregation kinetics of hematite were determined in a delicate work.[46] It was stated that at low ionic strengths, the rate constant is a function of pH and goes through a flat maximum around the point of zero charge (pzc), where fast aggregation conditions are reached, while at high ionic strength, the system is in the fast aggregation regime with pH independent rate constants. It should be mentioned here that the reproducibility of measured size data for colloidally stable systems was very good within ± 5 %, though the relation $qr_h << 1$ was not obviously fulfilled. In the aggregating suspensions, however, the measured particle size increased with time, showing the progress of coagulation. Therefore, the measured larger size data around the pH_{pzc} of magnetite for the fresh sample and all measured points of aged magnetite in Figure 7 are suitable only for comparing a given kinetic state of coagulating systems. Without demanding any details of colloidal stability, it is worth comparing the pH-dependent aggregation of fresh and aged magnetite samples, since their difference is obvious. The 6-year-old magnetite shows neither pH nor

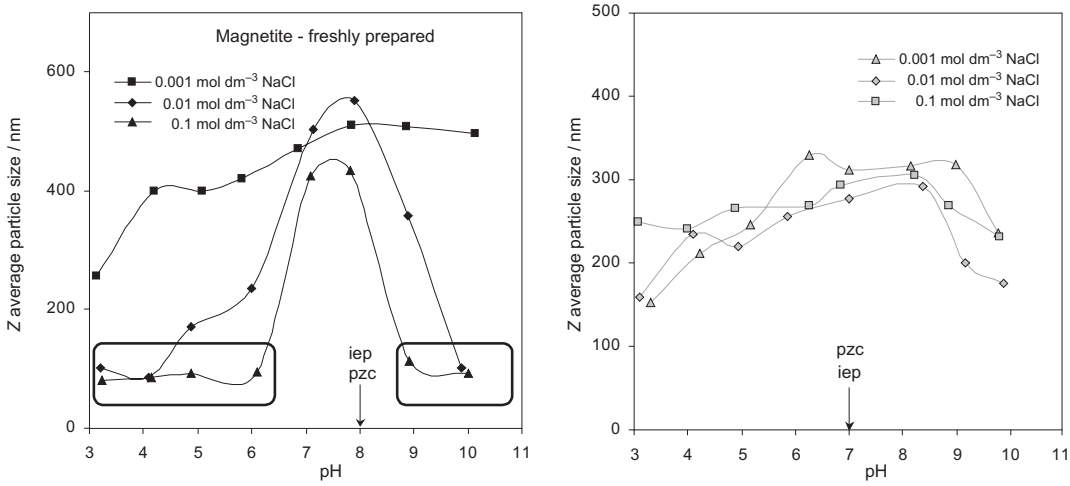

Figure 7. The pH-dependent aggregation in suspensions of fresh and aged magnetite nanoparticles.

ionic strength dependence. It seems that the aged sample lost entirely the feature of electrostatic stabilization during its long storage. This simple experimental finding is probably related to the storage problem of water based magnetic fluids.

CONCLUSIONS

As an interesting example of ageing in the inorganic nanoworld, changes in the inherent solid phase and the aqueous interfacial properties of magnetite nanoparticles in a Massart type magnetic fluid were presented in this work. The essence of the magnetic fluids is the superparamagnetic behavior of magnetic nanoparticles, which is closely related to the quality of crystallites, *i.e.,* their magnetic susceptibility, and their size compared to that of a single magnetic domain. While the solid phase transformation of magnetite to maghemite and a slight increase in particle size during 6 years of storage were proved in the present study, the superparamagnetic feature did not change after all, since the magnetic susceptibility of these iron oxides is not too different and the size limit of the single domain is still above the average size of particles measured after storage as long as 6 years. In contrast to the inner character, the outer properties at the aqueous interface underwent such a great alteration during the long storage time that the aged system cannot be called magnetic fluid any more because of the decline in colloidal stability. Besides the akageneite shell formation on the magnetite core, transformed partially to maghemite, surprisingly neither the surface charge density nor the particle charge in the acidic region showed a significant change, except for the definite decrease in the pH of pzc and iep (from pH ≈ 8 to ≈ 7). The ageing of synthetic magnetite formed as nanoparticles may be the reason for the different literature data of its surface charge characterization, since the Ostwald ripening in the nanosize region is faster due to enhanced dissolution, which is unfortunately often neglected in recent papers. The coalescence of akageneite shell during recrystallization resulted in a significant decrease in the specific surface area of the aged magnetite sample, and probably contributed to its declining colloidal stability.

Acknowledgements. – This work was supported by the Environmental Science and Chemistry Doctoral Schools, University of Szeged, and the Hungarian National Office of Research and Technology (NKTH-OTKA 69109, OMFB-01604/2006).

REFERENCES

1. D. J. Shaw, *Introduction to Colloid and Surface Chemistry*, Butterworths, London, 1980, p. 273.
2. D. H. Everett, *Basic Principles of Colloid Science*, RSC, London, 1988, p. 243.
3. R. J. Hunter, *Foundations of Colloid Science,* Vol. 1, Clarendon Press, Oxford, 1989, p. 673.
4. J. Lyklema, *Fundamentals of Interface and Colloid Science*, Vol. 1, *Fundamentals*, Academic Press, London, 1991. p. *ca.* 600.
5. W. Ostwald, *Z. Phys. Chem. (Leipzig)* **34** (1907) 295.
6. J. M. Bigham, R.W. Fritzpatrick, and D. G. Schulze, *Iron Oxides*, in: J. B. Dixon and D. G. Schulze (Eds.), *Soil Mineralogy with Environmental Applications*, SSSA, Madison, Wisconsin, USA, 2002, pp. 323–366.
7. R. M. Cornell and U. Schwertmann, *Iron Oxides in the Laboratory: Preparation and Characterization*, VCH, Weinheim, 1991.
8. R. M. Cornell and U. Schwertmann, *The iron oxides*, VCH, Weinheim, 1996, p. 573.
9. C. Scherer and A. M. Figueiredo Neto, *Brazilian J. Phys.* **35** (2005) 718–727.
10. Q. A. Pankhurst, J. Connolly, S. K. Jones, and J. Dobson, *J. Phys. D. Appl. Phys.* **36** (2003) R167–R181.
11. Z. Sun, F. Su, W. Forsling, and P. Samskog, *J. Colloid Interface Sci.* **197** (1998) 151–159.
12. Y. Sun, M. Ma, Y. Zhang, and N. Gu, *Colloids Surf., A* **245** (2004) 15–19.
13. E. Illés and E. Tombácz, *Colloids Surf., A* **230** (2003) 99–109.
14. E. Illés and E. Tombácz, *J. Colloid Interface Sci.* **295** (2006) 115–123.
15. P. Atkins and J. de Paula, *Atkins' Physical Chemistry*, Seventh Edition, *The solid state*, Oxford University Press, Oxford, 2002, pp. 767–777.
16. F. Bartram, *Crystallite-size determination from line broadening and spotty patterns*, in: E. F. Kaelble (Ed.), *Handbook of X-rays*, McGraw-Hill, New York, 1967, pp. 17.1.–17.18.
17. A. L. Patterson, *Phys. Rev.* **56** (1939) 978–982.
18. E. Tombácz and M. Szekeres, *Langmuir* **17** (2001) 1411–1419.
19. T. Chen, H. Xu, Q. Xie, J. Chen, J. Ji, and H. Lu, *Earth Planet. Sci. Lett.* **240** (2005) 790–802.
20. E. Murad and U. Schwertmann, *Clays Clay Miner.* **41** (1993) 111–113.
21. J. Tang, M. Myers, K. A. Bosnick, and L. E. Brus, *J. Phys. Chem. B* **107** (2003) 7501–7506.
22. R. M. Cornell, *Z. Pflanz. Bodenkunde* **155** (1992) 449–453.
23. H. Liu, Y. Wei, Y. Sun, and W. Wei, *Colloids Surf., A* **252** (2005) 201–205.
24. M. Kosmulski, *Chemical properties of material surfaces*, Marcel Dekker, New York, 2001, p. 753.
25. J. Lyklema, *Pure Appl. Chem.* **63** (1991) 895–906.
26. N. Kallay, Z. Dojnović, and A. Čop, *J. Colloid Interface Sci.* **286** (2005) 610–614.
27. T. Preočanin, A. Čop, and N. Kallay, *J. Colloid Interface Sci.* **299** (2006) 772–776.
28. R. O. James and G. A. Parks, *Characterization of Aqueous Colloids by Their Electrical Double-Layer and Intrinsic Surface Chemical Properties*, in: E. Matijevic (Ed.), *Surface and Colloid Science*, Vol. 12, Plenum, New York, 1982, pp. 119–216.
29. N. Marmier, A. Delisée, and F. Fromage, *J. Colloid Interface Sci.* **211** (1999) 54–60.

30. E. Tombácz, *Adsorption from electrolyte solutions*, in: J. Tóth (Ed.), *Adsorption: Theory, Modeling, and Analysis*, Marcel Dekker, New York, 2002, pp. 711–742.
31. N. Kallay, S. Žalac, and I. Kobal, *Problems in Modelling the Electrical Interfacial Layer in Metal/Oxide Aqueous Systems*, in: A. Dabrowski and V. A. Tertykh (Eds.), *Adsorption on New and Modified Inorganic Sorbents Studies in Surface Science and Catalysis*, Elsevier, Amsterdam, 1996, pp. 857–877.
32. M. Borkovec, B. Jönsson, and G. J. M. Koper, *Ionization processes and proton binding in polytropic systems: small molecules, proteins, interfaces and polyelectrolytes*, in: E. Matijevic (Ed.), *Surface and Colloid Science,* Vol. 16, Kluwer Academic/Plenum Press, Dordrecht, 2001, pp. 99–339.
33. M. Borkovec, *Langmuir* **13** (1997) 2608–2613.
34. A. Čop, D. Kovačević, T. Dragić, and N. Kallay, *Colloids Surf., A* **230** (2003) 159–165.
35. A. L. Herbelin and J. C. Westall, *FITEQL v.3.2.*, Oregon State University, Corvallis, OR, USA, 1996.
36. A. E. Regazzoni, M. A. Blesa, and A. J. G. Maroto, *J. Colloid Interface Sci.* **91** (1983) 560–570.
37. M. A. Blesa, N. M. Figliola, A. J. G. Maroto, and E. Regazzoni, *J. Colloid Interface Sci.* **101** (1984) 410–418.
38. R. J. Hunter, *Zeta Potential in Colloid Science, Principles and Applications*, Academic Press, London, 1981, p. 386.
39. H. Ohshima, *J. Colloid Interface Sci.* **275** (2004) 665–669.
40. H. Holthoff, S. U. Egelhaaf, M. Borkovec, P. Schurtenberger, and H. Sticher, *Langmuir*, **12** (1996) 5541–5548.
41. G. R. Wiese and T.W. Healy, *J. Colloid Interface Sci.* **51** (1975) 427–433.
42. E. Tombácz, M. Szekeres, I. Kertész, and L. Turi, *Progr. Colloid Polym. Sci.* **98** (1995) 160–168.
43. E. Tombácz, G. Filipcsei, M. Szekeres, and Z. Gingl, *Colloids Surf., A* **151** (1999) 233–244.
44. E. Tombácz, Cs. Csanaky, and E. Illés, *Colloid Polym. Sci.* **279** (2001) 484–492.
45. N. Kallay and S. Žalac, *J. Colloid Interface Sci.* **253** (2002) 70–76.
46. M. Schudel, S. H. Behrens, H. Holthoff, R. Kretzschmar, and M. Borkovec, *J. Colloid Interface Sci.* **196** (1997) 241–253.

SAŽETAK

Starenje u anorganskom nanosvijetu: nanočestice magnetita u vodenom mediju

Etelka Tombácz, Erzsébet Illés, Andrea Majzik, Angéla Hajdú, Nóra Rideg i Márta Szekeres

Istraživane su promjene svojstava nanočestica magnetita u čvrstom stanju i na međupovršini čvrsto/tekuće pomoću magnetske tekućine tipa Massart. Nanočestice magnetita sintetizirane su, pročišćene i dijalizirane pomoću 0,001 mol dm^{-3} HCl te ostavljene stajati 6 godina pri temperaturi od 4 °C. Dokazana je transformacija magnetita u maghemit i nastajanje sloja akaganeita na magnetskoj jezgri, kao i lagani porast veličine čestica, što nije utjecalo na promjenu superparamagnetskih svojstava nanočestica nakon stajanja od čak 6 godina. S druge strane, svojstva na međupovršini čvrsto/tekuće promijenila su se na čudan način. Iznenađujuće, niti površinska gustoća naboja niti naboj čestica u kiselom području nisu pokazali značajnu promjenu osim promjene pH_{pzc} i pH_{iep} od pH ≈ 8 do ≈ 7. Nastajanje sloja akaganeita tijekom rekristalizacije rezultiralo je značajnim smanjenjem specifične površine uzorka i vjerojatno pridonijelo smanjenju koloidne stabilnosti.